European Radiology (2024) 34:1836–1845
https://doi.org/10.1007/s00330-023-09972-8

European Radiology
EUROPEAN SOCIETY OF RADIOLOGY

CARDIAC

Impact of vessel morphology on CT-derived fractional-flow-reserve in non-obstructive coronary artery disease in right coronary artery

Toshimitsu Tsugu[1] · Kaoru Tanaka[1] · Dries Belsack[1] · Yuji Nagatomo[2] · Mayuko Tsugu[1] · Jean-François Argacha[3] · Bernard Cosyns[3] · Nico Buls[1] · Michel De Maeseneer[1] · Johan De Mey[1]

Received: 20 February 2023 / Revised: 16 May 2023 / Accepted: 28 May 2023 / Published online: 1 September 2023

Abstract

Objectives Computed tomography (CT)–derived fractional flow reserve (FFR_{CT}) decreases continuously from proximal to distal segments of the vessel due to the influence of various factors even in non-obstructive coronary artery disease (NOCAD). It is known that FFR_{CT} is dependent on vessel-length, but the relationship with other vessel morphologies remains to be explained.

Purpose To investigate morphological aspects of the vessels that influence FFR_{CT} in NOCAD in the right coronary artery (RCA).

Methods A total of 443 patients who underwent both FFR_{CT} and invasive coronary angiography, with < 50% RCA stenosis, were evaluated. Enrolled RCA vessels were classified into two groups according to distal FFR_{CT}: $FFR_{CT} \leq 0.80$ ($n = 60$) and $FFR_{CT} > 0.80$ ($n = 383$). Vessel morphology (vessel length, lumen diameter, lumen volume, and plaque volume) and left-ventricular mass were assessed. The ratio of lumen volume and vessel length was defined as V/L ratio.

Results Whereas vessel-length was almost the same between $FFR_{CT} \leq 0.80$ and > 0.80, lumen volume and V/L ratio were significantly lower in $FFR_{CT} \leq 0.80$. Distal FFR_{CT} correlated with plaque-related parameters (low-attenuation plaque, intermediate-attenuation plaque, and calcified plaque) and vessel-related parameters (proximal and distal vessel diameter, vessel length, lumen volume, and V/L ratio). Among all vessel-related parameters, V/L ratio showed the highest correlation with distal FFR_{CT} ($r = 0.61$, $p < 0.0001$). Multivariable analysis showed that calcified plaque volume was the strongest predictor of distal FFR_{CT}, followed by V/L ratio (β-coefficient = 0.48, $p = 0.03$). V/L ratio was the strongest predictor of a distal $FFR_{CT} \leq 0.80$ (cut-off 8.1 mm^3/mm, AUC 0.88, sensitivity 90.0%, specificity 76.7%, 95% CI 0.84–0.93, $p < 0.0001$).

Conclusions Our study suggests that V/L ratio can be a measure to predict subclinical coronary perfusion disturbance.

Clinical relevance statement A novel marker of the ratio of lumen volume to vessel length (V/L ratio) is the strongest predictor of a distal CT-derived fractional flow reserve (FFR_{CT}) and may have the potential to improve the diagnostic accuracy of FFR_{CT}.

Key Points

- *Physiological FFR_{CT} decline depends not only on vessel length but also on the lumen volume in non-obstructive coronary artery disease in the right coronary artery.*
- *FFR_{CT} correlates with plaque-related parameters (low-attenuation plaque, intermediate-attenuation plaque, and calcified plaque) and vessel-related parameters (proximal and distal vessel diameter, vessel length, lumen volume, and V/L ratio).*
- *Of vessel-related parameters, V/L ratio is the strongest predictor of a distal FFR_{CT} and an optimal cut-off value of 8.1 mm^3/mm.*

Keywords Coronary artery disease · Computed tomography angiography · Ischemia

✉ Toshimitsu Tsugu
ttsugu@uzbrussel.be

[1] Department of Radiology, Universitair Ziekenhuis Brussel, Laarbeeklaan 101, 1090 Jette, Brussels, Belgium

[2] Department of Cardiology, National Defense Medical College Hospital, Tokorozawa, Japan

[3] Cardiology, Centrum Voor Hart- en Vaatziekten, Universitair Ziekenhuis Brussel, Brussels, Belgium

Abbreviations

CAD	Coronary artery disease
CAD-RADS	CAD reporting and data system
CP	Calcified plaque
CTA	CT angiography
FFR	Fractional flow reserve
FFR_{CT}	Computed tomography–derived fractional flow reserve
HU	Hounsfield units

IAP	Intermediate-attenuation plaque
ICA	Invasive coronary angiography
LAD	Left anterior descending artery
LAP	Low-attenuation plaque
LCX	Left circumflex artery
LV	Left ventricular
NOCAD	Non-obstructive CAD
RCA	Right coronary artery

Introduction

Computed tomography (CT)–derived fractional flow reserve (FFR_{CT}) is a feasible tool for assessing the hemodynamic significance of coronary stenosis non-invasively with a high diagnostic accuracy of 81.9% [1]. The implementation of FFR_{CT} can change treatment strategies and improve diagnostic efficiency and effectiveness in patients with coronary artery disease (CAD) [2]. Even in non-obstructive CAD (NOCAD), FFR_{CT} gradually decreases from the proximal to the distal segments of the vessel (physiological FFR_{CT} decline) [3, 4]. FFR_{CT} is influenced by various factors such as vessel length [3, 4], bifurcation angle [5, 6], plaque burden [3], left ventricular mass [7], and collateral circulation [8]. FFR_{CT} is modified by multiple variables, resulting in 37% of vessels presenting FFR_{CT} of ≤ 0.80 even with normal coronary arteries [9]. Vessel length plays an important role in physiological FFR_{CT} decline [3, 4]. It is empirically proven that differing FFR_{CT} changes occur depending on the lumen volume even with the same vessel length. The lumen cross-sectional area decreases towards the distal segments [10], resulting in vessel tapering. The lumen cross-sectional area correlates with FFR_{CT} [11]. Furthermore, with a higher dose of nitroglycerin as a vasodilator agent, lumen volume increases, resulting in FFR_{CT} elevation at the distal vessel segments [12]. Hence, physiological FFR_{CT} decline may be related to lumen volume [9]. The relationship between vessel length and lumen volume and FFR_{CT} remains to be explained. The present study aimed to investigate morphological aspects of the vessels and to identify predictive factors forphysiological FFR_{CT} decline in NOCAD in the right coronary artery (RCA).

Methods

Patient population

A total of 1624 outpatients with suspected CAD and who had a CT angiography (CTA) with FFR_{CT} analysis examined at the Universitair Ziekenhuis Brussel between January 2017 and January 2023 were included in the study. A retrospective cohort study was performed. Approval from the ethical board at the Universitair Ziekenhuis Brussel was obtained with protocol number B.U.N. 143202000302. Inclusion criteria were NOCAD on ICA at the RCA. The presence of coronary stenosis in the left coronary artery was irrelevant. NOCAD was defined as vessels with < 50% coronary stenosis or luminal irregularities. The severity of coronary stenosis on CTA was determined as 0–2 according to CAD reporting and data system (CAD-RADS) classification [13] by experts in cardiac radiology imaging (T.T., and K.T.). The severity of coronary stenosis was assessed visually by experienced interventional cardiologists (JF.A. and C.B.). A total of 838 patients who had not undergone ICA and 133 patients with ≥ 50% coronary stenosis were excluded from the study. Although not included in the current study, patients with heart failure and old myocardial infarction were excluded. The following categories of patients were also excluded from the study: time interval between FFR_{CT} and ICA > 90 days ($n = 77$), RCA anomaly (hypoplasia, anomalous origin) ($n = 68$), inappropriate image quality (motion artifact, blooming artifact, or noise artifact) ($n = 44$), post transcatheter aortic valve implantation ($n = 6$), myocardial bridge ($n = 4$), post coronary artery bypass graft ($n = 2$). As a result, 443 patients were enrolled and divided into two groups according to RCA distal vessel FFR_{CT}: FFR_{CT} ≤ 0.80 ($n = 60$) and FFR_{CT} > 0.80 ($n = 383$). The patient selection flowchart is presented in Fig. 1.

Coronary CT angiography

All coronary CTA scans were acquired with a 320 slice GE Revolution scanner (GE Healthcar) enabling to image the heart in one heartbeat. This protocol used a single-rotation axial scan with prospective gating, 16-cm detector coverage, noise index 30 (noise level fixed over all kVp levels and body sizes), and gantry rotation time of 0.28 s. Tube potential ranged between 70 and 120 kV depending on body size. Iodinated contrast agent was administered with Iopromide 370 (Bayer Schering Pharma) using the bolus tracking method at a rate of 5.0 ml/s depending on body size. The volume of iodinated contrast injected was individualised according to body size (50–80 mL). Beta-blockers were administered when necessary to obtain a target heart rate of < 60 beats/min. According to guidelines [14], sublingual nitrates (two sprays of 0.8 mg) were administered 5 min prior to CT scanning in all patients. The images were reconstructed at 75 ± 10% of the R-R interval.

FFR_{CT}

FFR_{CT} was analysed by HeartFlow Inc. Computational fluid dynamics and blood flow simulations were performed to calculate the FFR_{CT} at any arbitrary point in the coronary artery. The RCA was classified into 4 segments (#1–#4) based on the American Heart Association classification (AHA) [15]. To avoid the effects of turbulence due to branching, FFR_{CT}

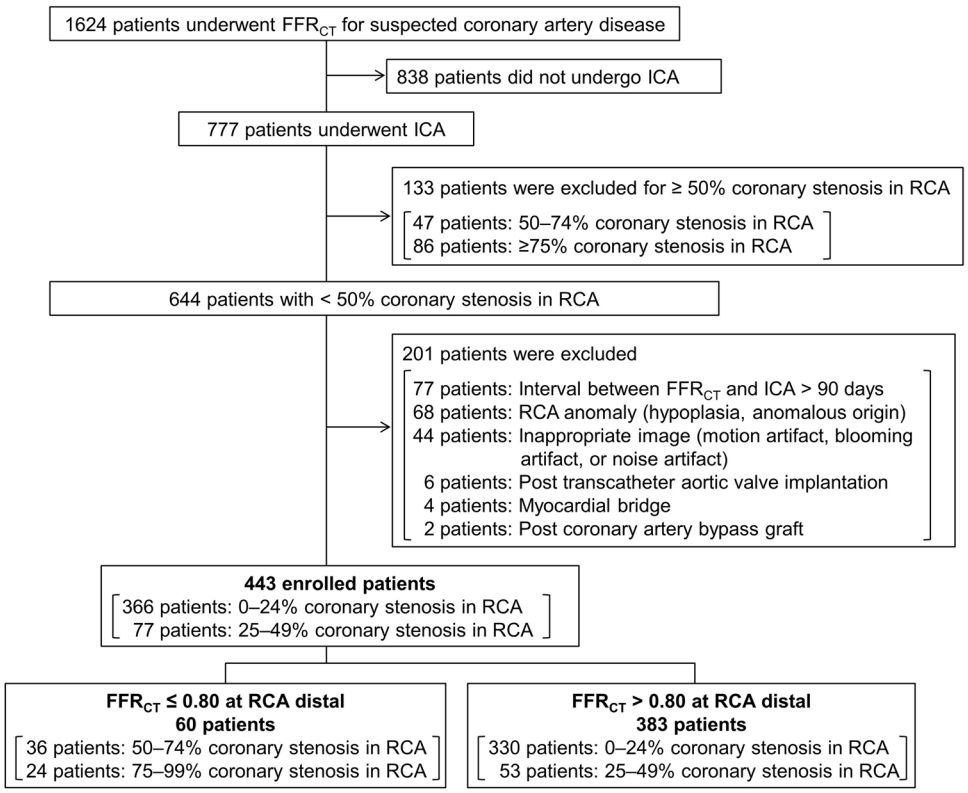

Fig. 1 Patient selection flow diagram showing patient flow in the study. CTA, computed tomography angiography; ICA, invasive coronary angiography; RCA, right coronary artery

values were measured from RCA ostium (#1) to the bifurcation (#3 distal end) of the atrioventricular nodal branch (#4AV) and posterior descending branch (#4PD) (Fig. 2). Moreover, each segment was divided into three categories (proximal, middle, and distal). The magnitude of change in FFR_{CT} (ΔFFR_{CT}) was measured from the proximal to the distal at the RCA. A positive FFR_{CT} was defined as a value ≤ 0.80 in accordance with previously published literature [16–19].

Coronary artery morphology and composition

Vessel diameter, vessel length, lumen volume, and composition of each vessel were measured using GE AW server 3.2 software (GE Healthcare). The ratio of lumen volume and vessel length was defined as V/L ratio (mm^3/mm). Plaque characterisation and vessel morphology measurements were performed semi-automatically with Color Code Plaque (GE Healthcar). Vessel constituents were characterised based on Hounsfield units (HU) into low-attenuation plaque (LAP) (< 30 HU), intermediate-attenuation plaque (IAP) (30–150 HU), and calcified plaque (CP) (> 150 HU) [20, 21].

Invasive coronary angiography

All ICA images were evaluated by Philips Azurion with ClarityIQ (Philips Healthcare). Iodixanol 320 (GE Healthcare) was administered as an iodinated contrast agent.

Statistical analysis

Continuous variables were expressed as mean ± standard deviation (SD). The 95% confidence interval was calculated as ± 1.96 SDs from the mean. Two groups ($FFR_{CT} > 0.80$ and ≤ 0.80) comparisons were performed with paired t test or 1-way analysis of variance for means if the data were normally distributed or with Mann–Whitney *U* test or Kruskal–Wallis test if the data were not normally distributed. Fisher's or χ^2 test was used to analyse the categorical data. Associations between distal FFR_{CT}, ΔFFR_{CT}, and cardiac parameters were assessed by Pearson correlation analysis. Multivariable linear regression analyses were performed to examine the independent correlates between distal FFR_{CT}, ΔFFR_{CT}, and cardiac parameters. Receiver operating characteristic curves and their area under the curve were estimated based on Mann–Whitney U test, and the null hypothesis on the area under the curve C (H0: area under the curve = 0.5) was tested. Receiver operating characteristics curves were generated to determine the cut-off value of the highest diagnostic performance of an $FFR_{CT} \leq 0.80$ at the distal vessel. Intra-observer (T.T.) and inter-observer (T.T. and K.T.) agreement was assessed in 15 randomly selected subjects using Bland–Altman analyses. $p < 0.05$ was considered statistically significant. All statistical analyses were performed with JMP 11.0 statistical software (SAS Institute) or R version 4.4.2 (R Foundation for Statistical Computing).

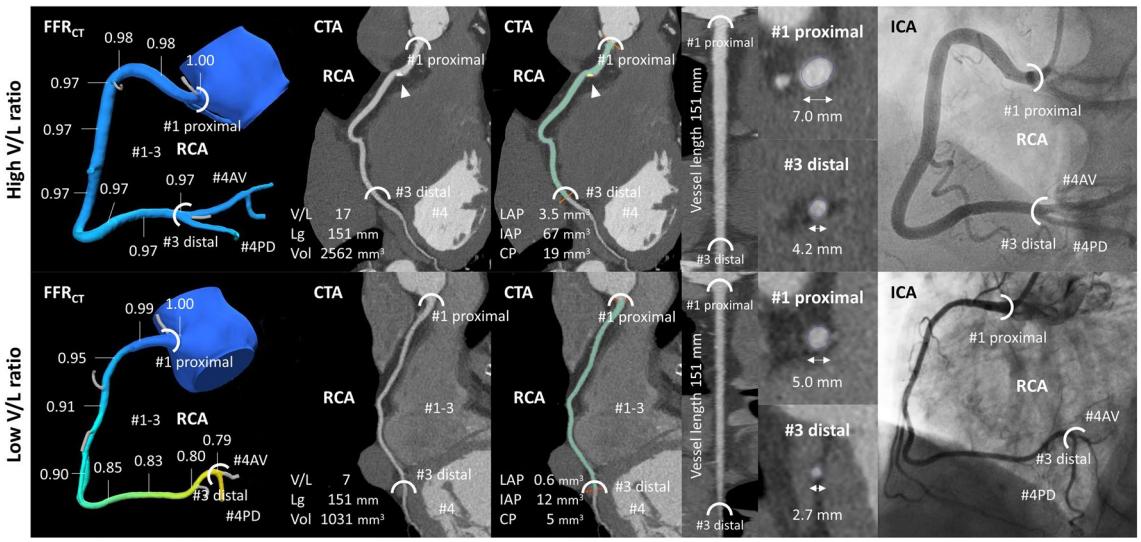

Fig. 2 Representative cases of high V/L ratio (top panel) and low V/L ratio (bottom panel). Analysis range is from #1 proximal to #3 distal. Arrowhead (CP). AV, atrioventricular nodal; CP, calcified plaque; IAP, intermediate-attenuation plaque; LAP, low-attenuation plaque; Lg, vessel length; PD, posterior descending; Vol, lumen volume

Results

Physical, CT acquisition condition, FFR_{CT}, and vessel characteristics

Among 443 patients, 383 patients (86%) had $FFR_{CT} > 0.80$, whereas 60 patients (14%) showed a positive FFR_{CT} even in NOCAD in the RCA (Fig. 3). Table 1 summarises the physical, CT acquisition condition, FFR_{CT}, vessel, and myocardial characteristics in the RCA in our study population. Physical characteristics did not differ between $FFR_{CT} \leq 0.80$ and > 0.80. The time phase in the cardiac cycle during CT images could be acquired at the mid-diastolic phase in all patients. Proximal FFR_{CT} was identical between $FFR_{CT} \leq 0.80$ and > 0.80, but distal FFR_{CT} (0.72 ± 0.09 vs. 0.90 ± 0.04, $p < 0.0001$) and ΔFFR_{CT} (0.28 ± 0.09 vs. 0.10 ± 0.04, $p < 0.0001$) were significantly lower in $FFR_{CT} \leq 0.80$ than in > 0.80 (Fig. 4, Table 1, and Supplementary Table 1). Vessel length did not differ between $FFR_{CT} \leq 0.80$ and > 0.80 (118.3 ± 22.3 vs. 113.4 ± 17.4 mm, $p = 0.11$). Proximal vessel diameter, distal vessel diameter, lumen volume (825.7 ± 255.0 vs. 1113.0 ± 337.9 mm^3, $p < 0.0001$), and V/L ratio (6.5 ± 1.6 vs. 9.9 ± 2.4 mm^3/mm, $p < 0.0001$) were significantly lower in $FFR_{CT} \leq 0.80$ than in > 0.80. Vessel length was almost the same, but vessel morphology (proximal vessel diameter, distal vessel diameter, lumen

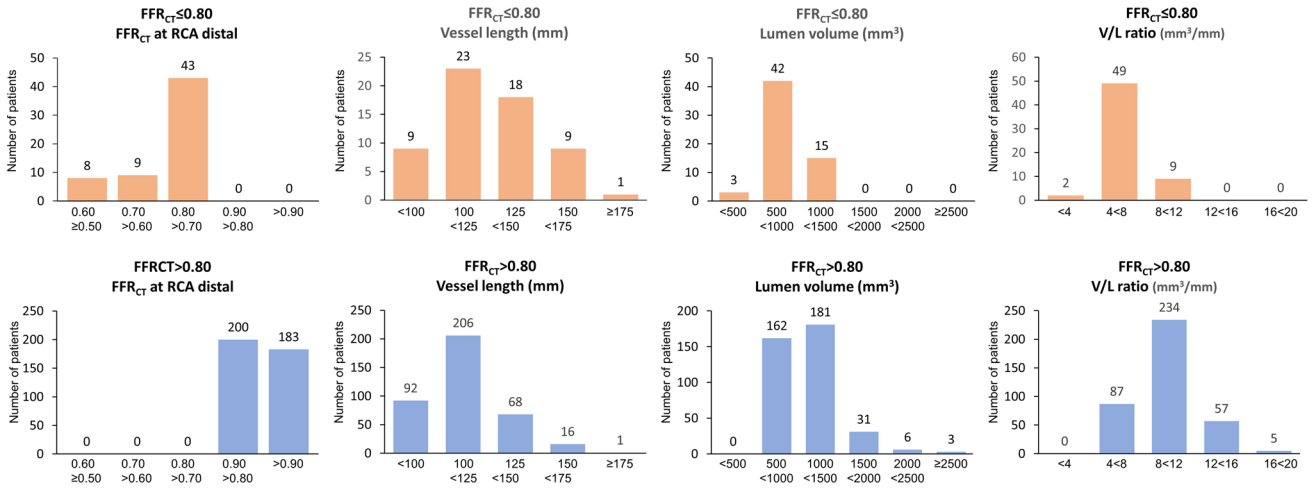

Fig. 3 Distribution of FFR_{CT} and vessel morphology

Table 1 Physical, CT acquisition condition, FFR_{CT}, vessel, and myocardial characteristics in the right coronary artery

	All $n=443$	$FFR_{CT} \leq 0.80$ $n=60$	$FFR_{CT} > 0.80$ $n=383$
Physical characteristics			
Age (years)	67.2 ± 9.9	69.3 ± 7.8	66.9 ± 10.2
Men, *n* (%)	304 (69%)	36 (60%)	310 (81%)
Height (cm)	172.6 ± 9.5	171.4 ± 11.2	172.8 ± 9.2
Body weight (kg)	81.0 ± 15.2	77.7 ± 17.2	81.5 ± 14.8
Body surface area (m^2)	1.9 ± 0.2	1.9 ± 0.3	1.9 ± 0.2
Body mass index (kg/m^2)	27.1 ± 4.3	26.2 ± 4.3	27.2 ± 4.3
Hypertension, *n* (%)	92 (51%)	11 (58%)	81 (51%)
Dislipidemia, *n* (%)	73 (41%)	8 (42%)	65 (41%)
Diabetes, *n* (%)	33 (19%)	5 (26%)	28 (18%)
Current smoking, *n* (%)	57 (32%)	7 (35%)	50 (31%)
CT images acquisition condition			
Time phase in the cardiac cycle during CT imaging	75.0 ± 5.4	74.7 ± 4.6	75.1 ± 5.5
Heart rate (beats/min)	60.3 ± 8.6	62.5 ± 9.2	59.9 ± 8.5
Atrial fibrillation, *n* (%)	46 (10%)	7 (12%)	39 (10%)
Systolic blood pressure (mmHg)	143.8 ± 19.8	147.2 ± 10.9	142.3 ± 19.3
Diastolic blood pressure (mmHg)	83.1 ± 12.1	87.8 ± 12.8	82.4 ± 11.9
Interval between FFR_{CT} and invasive coronary angiography (days)	22.0 ± 18.4	21.0 ± 15.0	22.1 ± 18.8
FFR_{CT} characteristics			
Proximal FFR_{CT}	1.00 ± 0.00	1.00 ± 0.00	1.00 ± 0.00
Distal FFR_{CT}	0.88 ± 0.08	0.72 ± 0.09†	0.90 ± 0.04
ΔFFR_{CT}	0.12 ± 0.08	0.28 ± 0.09†	0.10 ± 0.04
Vessel morphology			
Vessel length (mm)	114.0 ± 18.1	118.3 ± 22.3	113.4 ± 17.4
Lumen volume (mm^3)	1074.0 ± 342.3	825.7 ± 255.0†	1113.0 ± 337.9
Proximal vessel diameter (mm)	4.5 ± 1.0	3.9 ± 0.8†	4.6 ± 1.0
Distal vessel diameter (mm)	2.8 ± 0.6	2.4 ± 0.5†	2.9 ± 0.6
V/L ratio (mm^3/mm)	9.4 ± 2.6	6.5 ± 1.6†	9.9 ± 2.4
LAP volume (mm^3)	15.6 ± 18.5	18.6 ± 18.0	15.1 ± 18.6
IAP volume (mm^3)	156.6 ± 174.9	224.7 ± 194.5†	145.9 ± 169.4
CP volume (mm^3)	29.6 ± 68.2	67.7 ± 89.9†	23.6 ± 62.2
Myocardial morphology			
LV mass (g)	109.6 ± 31.9	107.6 ± 31.2	109.8 ± 32.0
LV mass index (g/m^2)	56.0 ± 14.6	57.4 ± 15.8	55.8 ± 14.4

CP, calcified plaque; *IAP*, intermediate-attenuation plaque; *LAP*, low-attenuation plaque; *LV*, left ventricular
*$p < 0.05$ vs. $FFR_{CT} > 0.80$. †$p < 0.01$ vs. $FFR_{CT} > 0.80$

volume, and V/L ratio) was significantly lower in $FFR_{CT} \leq 0.80$. Distal FFR_{CT} was lower in $\leq FFR_{CT} > 0.80$. LAP volume was almost the same comparing $FFR_{CT} \leq 0.80$ and > 0.80, but IAP and CP volume were higher in $FFR_{CT} \leq 0.80$ (Table 1).

Effects of RCA branches on FFR_{CT}

To investigate the effects of RCA branches on FFR_{CT}, changes in FFR_{CT} were compared in the following groups: (1) presence of both right ventricular branch and acute marginal branch confirmed by FFR_{CT} ($n = 305$); (2) presence of right ventricular branch confirmed by FFR_{CT} ($n = 99$); (3) presence of acute marginal branch confirmed by FFR_{CT} ($n = 28$); (4) absence of both right ventricular branch and acute marginal branch confirmed by FFR_{CT} ($n = 11$). Distal FFR_{CT} (group 1, 0.87 ± 0.08; group 2, 0.88 ± 0.08; group 3, 0.88 ± 0.06, and group 4, 0.89 ± 0.03) and ΔFFR_{CT} (group 1, 0.13 ± 0.08; group 2, 0.12 ± 0.08; group 3, 0.12 ± 0.06, and group 4, 0.11 ± 0.03) did not significantly differ between the four groups (Supplementary Table 2).

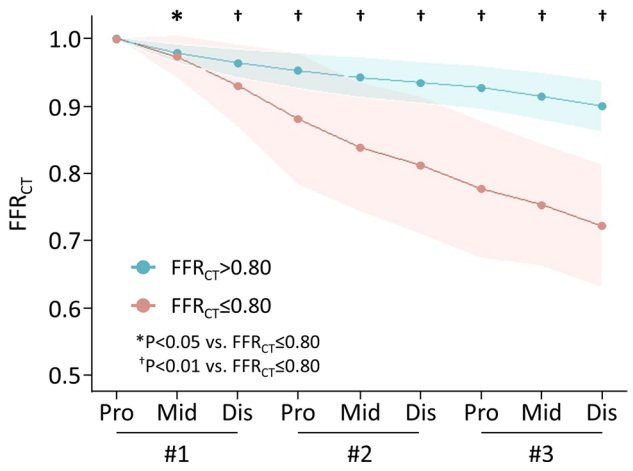

Fig. 4 Changes in FFR_{CT} between $FFR_{CT} \leq 0.80$ and > 0.80

Univariate and multivariate analysis of the relationship between FFR_{CT} and vessel morphology

In all patients ($FFR_{CT} \leq 0.80$ and > 0.80), distal FFR_{CT} and ΔFFR_{CT} were correlated with vessel-related parameters (proximal and distal vessel diameters, vessel length, lumen diameter, and V/L ratio) and plaque-related parameters (LAP, IAP, and CP volume). Among all vessel-related parameters, V/L ratio showed the highest correlation with distal FFR_{CT} ($r = 0.61$, $p < 0.0001$) (Fig. 5 and Supplementary Table 3) and ΔFFR_{CT} ($r = -0.61$, $p < 0.0001$) (Supplementary Fig. 1 and Supplementary Table 4). Multivariable analysis showed that CP volume was the strongest predictor of distal FFR_{CT} (β-coefficient $= -0.12$, $p = 0.01$), followed by V/L ratio (β-coefficient $= 0.48$, $p = 0.03$) (Table 2). Furthermore, as for ΔFFR_{CT}, CP plaque volume (β-coefficient $= 0.12$, $p = 0.01$) was the strongest predictor, and was followed by V/L ratio (β-coefficient $= -0.48$. $p = 0.03$) (Supplementary Table 5). Among vessel-related parameters, V/L ratio of 8.1 mm^3/mm had the highest diagnostic performance for an FFR_{CT} at distal RCA ≤ 0.80 (AUC = 0.88, 95% CI 0.84–0.93, $p <$ 0.0001, sensitivity 90.0%, specificity 76.7%) (Fig. 6 and Supplementary Table 6).

Repeatability and reproducibility

Intra-observer and inter-observer variability for vessel-related parameters and myocardium-related parameters is summarised in Supplementary Figs. 2 and 3. Intra-observer and inter-observer analyses showed good repeatability and reproducibility.

Discussion

In patients with an ICA showing no or minimal CAD in the RCA, our study highlighted the following: (1) vessel length was almost the same in $FFR_{CT} \leq 0.80$ and > 0.80, but lumen volume and V/L ratio were significantly lower in the $FFR_{CT} \leq 0.80$ group; (2) FFR_{CT} correlated with

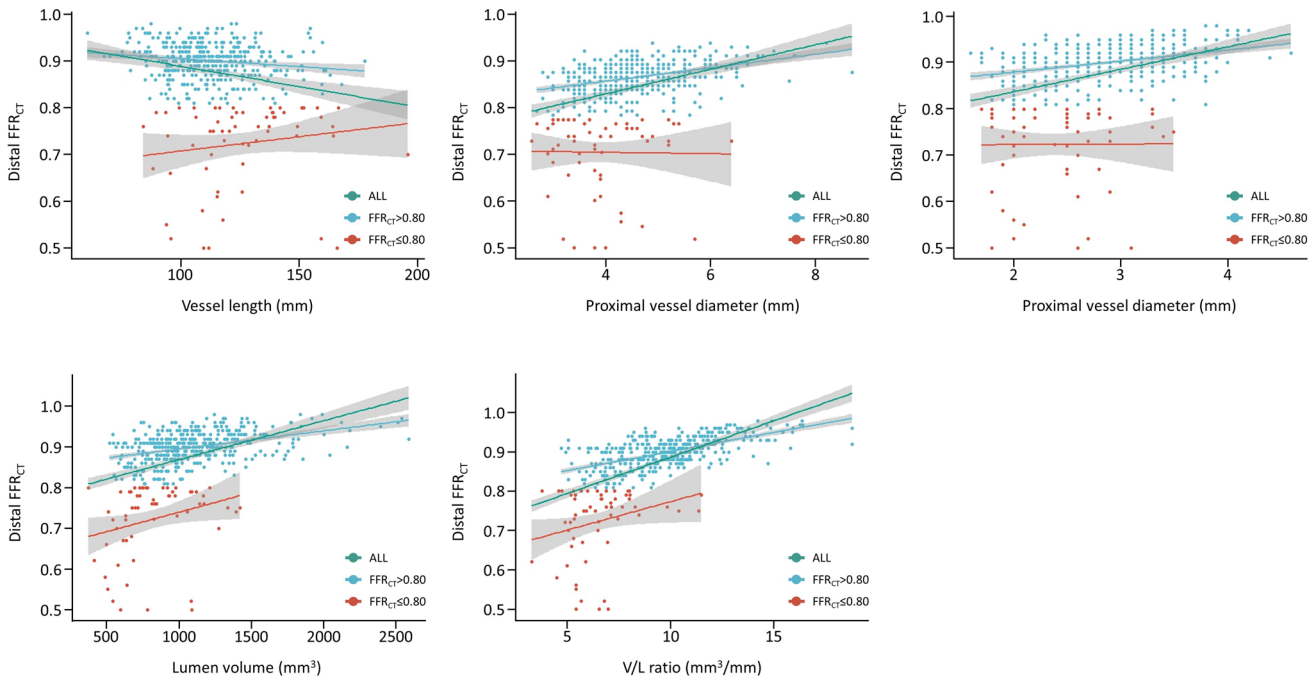

Fig. 5 Relationship between distal FFR_{CT} and vessel morphology

Table 2 Univariable and multivariable analysis for distal FFR_{CT}

	Univariable analysis				Multivariable analysis			
	β	95% CI	t-value	*p*-value	β	95% CI	t-value	*p*-value
Vessel length	−0.22	−0.001 to −0.0005	−4.70	<0.0001				
Lumen volume	0.42	0.00008 to 0.001	9.82	<0.0001				
Proximal vessel diameter	0.36	0.02 to 0.04	8.18	<0.0001	0.09	0.0002 to 0.01	2.02	0.04
Distal vessel diameter	0.37	0.04 to 0.06	8.37	<0.0001				
V/L ratio	0.61	0.016 to 0.02	16.30	<0.0001	0.48	0.001 to 0.03	2.14	0.03
LAP volume	−0.16	−0.0003 to −0.04	−3.30	0.001				
IAP volume	−0.17	−0.0001 to 0.00003	−3.51	0.0005				
CP volume	−0.19	−0.0003 to −0.0001	−4.09	<0.0001	−0.12	−0.0002 to −0.00003	−2.54	0.01
LV mass index	−0.07	−0.0009 to 0.0002	−1.32	0.19				

CI, confidence interval; *CP*, calcified plaque; *IAP*, intermediate-attenuation plaque; *LAP*, low-attenuation plaque; *LV*, left ventricular

plaque-related parameters (LAP, IAP, and CP) and vessel-related parameters (proximal and distal vessel diameter, vessel length, lumen volume, and V/L ratio); (3) of all parameters (plaque-related parameters and vessel related-parameters), the strongest predictor of a distal FFR_{CT} value was CP volume followed by V/L ratio and an optimal cut-off value of 8.1 mm^3/mm. Our study reports for the first time that FFR_{CT} decline depends on V/L ratio in patients with NOCAD in the RCA.

The progressive and continuous FFR_{CT} [3, 4] and invasive FFR [22] decline from the proximal to the distal segments of the vessel even in NOCAD is a commonly observed radiological finding. In our study, 60 patients (14%) with NOCAD had $FFR_{CT} < 0.80$. Physiological FFR_{CT} decline

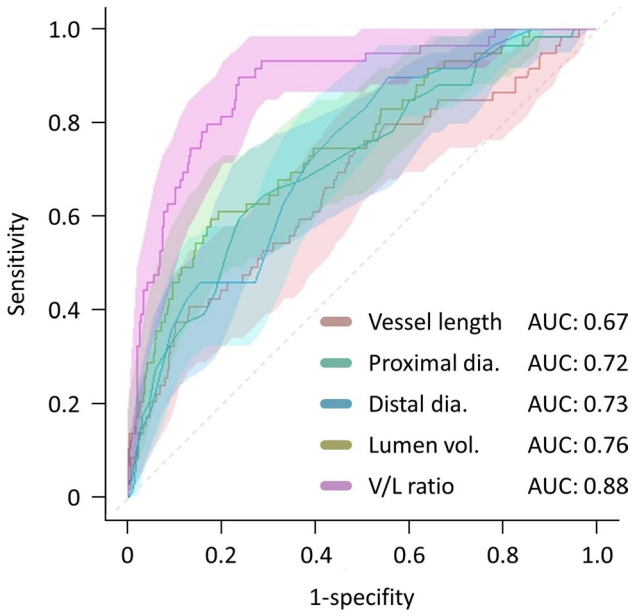

Fig. 6 Receiver operating curve of vessel morphology for predicting distal FFR_{CT}. dia., diameter; vol., volume

was dependent on iodine contrast attenuation and the full algorithm remains unclear for commercial reasons. However, FFR_{CT} hemodynamics have been reported to be influenced by various factors The degree of FFR_{CT} decline was not hemodynamically uniform in major three vessels and that RCA was smaller than LAD and LCX. This finding may be related to energy loss due to turbulence by the bifurcation from the left main trunk to LAD and LCX, or splitting into large branches such as diagonal branch, obtuse marginal branch, or posterior descending branch. Our previous study on the ramus artery demonstrated that the presence of a large ramus artery yields energy loss due to turbulence around the bifurcation angle, resulting in distal FFR_{CT} decline in both LAD and LCX [23, 24]. Turbulent eddies generated by the presence of large branches could contribute to energy loss, resulting in impact on FFR_{CT} hemodynamics. RCA may also have side branches such as the right ventricular branch or acute marginal branch (Supplementary Table 2). Turbulence flow generated in the RCA side branches was small and unlikely to affect FFR_{CT}. Therefore, RCA with no major branches was included in the present study.

The finding that the degree of FFR_{CT} decline depended on vessel length was consistent with previous reports [3, 4]. Interestingly, even though vessel length was almost the same between $FFR_{CT} \leq 0.80$ and > 0.80, proximal/distal vessel diameters, lumen volume, and V/L ratio were significantly lower in $FFR_{CT} \leq 0.80$. Vessel morphology including proximal/distal vessel diameters, lumen volume, and V/L ratio may have the potential to play an important role in physiological FFR_{CT} hemodynamics. Several studies have reported the effects of vessel morphology on FFR_{CT} from two perspectives: luminal cross-sectional area (2D) and vessel volume (3D). At the 2D level (luminal cross-sectional area), Collet et al [11] reported that FFR_{CT} was significantly correlated with the luminal cross-sectional area. At the 3D level (lumen volume), Holmes et al [12] reported that increase in homogeneous lumen volume caused by the vasodilator agent

of nitroglycerin resulted in FFR_{CT} elevation. According to Hagen-Poiseuille flow, the change in pressure is proportional to the length, and the volumetric flow rate, and inversely proportional to the fourth power of the lumen diameter radius [25]. Baumgartner et al [26] reported that positive remodelling which was heterogeneous vasodilatation was associated with an increase in FFR_{CT}. The streamlined vessel morphology caused by positive remodelling leads to pressure recovery phenomena, which may be responsible for the FFR_{CT} elevation. Tapering as a morphological change of the vessel might contribute to FFR_{CT} decline. A small distal vessel diameter was related to $FFR_{CT} \leq 0.80$ at the distal segment [9]. Our results of multivariable analysis were consistent with the results of previous studies. Of the vessel morphology-related parameters, V/L ratio was the most predictive factor for distal FFR_{CT}. Hence, a thinner and longer vessel contributes to a larger FFR_{CT} decline. Conversely, a shorter and thicker vessel causes a smaller FFR_{CT} decline.

Differences between $FFR_{CT} \leq 0.80$ and > 0.80 could be attributed to hemodynamic stress. FFR_{CT} depends on coronary artery flow. Coronary artery flow is determined by hemodynamic stress following three factors: (1) wall shear stress; (2) perfusion pressure; (3) vascular resistance. Of these factors, wall shear stress is affected by vessel diameter (inversely related to vessel diameter). Wall shear stress generates nitric oxide, which increases coronary artery flow, resulting in greater pressure drop and FFR_{CT} decline [27]. In our study, $FFR_{CT} \leq 0.80$ group tended to have smaller vessel diameters than > 0.80, which might contribute to high shear stress and small FFR_{CT} values. To our knowledge, this is the first report to investigate the effect of the ratio of lumen volume to vascular length on FFR_{CT}. The addition of a novel parameter, V/L ratio assessment in addition to the conventional FFR_{CT} interpretation may have the potential to overcome some drawbacks of FFR_{CT}. Decision making based on FFR_{CT} values at distal coronary artery segments should be performed with the greatest caution and by a thorough consideration of lumen volume.

Limitations

Our study has some limitations. First, invasive FFR was not performed because included patients were NOCAD. Since FFR_{CT} is highly concordant with invasive FFR, it can be used as an alternative testing method [28–30]. Our study excluded a history of old myocardial infarction, but may not have completely ruled out the effects of left coronary artery disease. Old myocardial infarction causes left ventricular (LV) dysfunction, resulting in reduced left ventricular myocardial–related parameters such as LV wall thickness or LV mass. Fairbairn et al reported that the ratio of lumen volume to LV mass (V/M ratio) and FFR_{CT} were inversely related. In our previous study, LV mass index was the most influential factor on FFR_{CT} among LV myocardial-related parameters, with a cut-off value of 66.5 g/m^2. Furthermore, LV dysfunction due to old myocardial infarction or heart failure causes an increase in LV end-diastolic pressure or low cardiac output, resulting in a decrease in right ventricular perfusion. In the setting of low right ventricular perfusion, the pressure drop is lower than normally expected coronary blood flow, resulting in higher FFR_{CT} values. Collateral circulation generates unusual coronary hemodynamics from donor artery perfusion. FFR_{CT} values depend on the donor and recipient arteries balance (Supplementary Fig. 4). In our study, patients with old myocardial infarction or heart failure were excluded, and it is unlikely that right ventricular perfusion would be compromised due to low cardiac output. LV mass index was below the threshold to affect FFR_{CT} hemodynamics and was not a strong predictor of distal FFR_{CT} and Δ FFR_{CT} in multivariate analysis. Furthermore, there was no evidence of collateral circulation. Therefore, left coronary artery disease was unlikely to affect FFR_{CT} in the RCA. Second, this study focused on only RCA vessels to avoid the effects of energy loss due to the bifurcation branches. Our results should be confirmed with all vessels including left coronary arteries. Third, despite the fact that FFR_{CT} is affected by plaque volume [3, 31–33], this study did not completely eliminate plaque volume even though only NOCAD were selected. However, it is controversial to investigate FFR_{CT} in simulated vessel models that completely eliminates the effects of plaque characteristics. Simulated vessel models are assumed to have a rigid wall rather than an elastic wall; therefore, the simulation does not reflect the physiological situation [34].

Conclusions

A novel marker for the predictor of distal FFR_{CT}, V/L ratio is useful in assessing the physiological changes in subclinical perfusion disturbance in coronary arteries.

Supplementary information The online version contains supplementary material available at https://doi.org/10.1007/s00330-023-09972-8.

Funding The authors state that this work has not received any funding.

Declarations

Guarantor The scientific guarantor of this publication is Johan De Mey.

Conflict of interest The authors of this manuscript declare no relationships with any companies whose products or services may be related to the subject matter of the article.

Statistics and biometry No complex statistical methods were necessary for this paper.

Informed consent Written informed consent was obtained from all subjects (patients) in this study.

Ethical approval Universitair Ziekenhuis Brussel Institutional Review Board (B.U.N. 143202000302) approval was obtained.

Study subjects or cohorts overlap None.

Methodology
- retrospective
- observational
- performed at one institution

References

1. Cook CM, Petraco R, Shun-Shin MJ et al (2017) Diagnostic accuracy of computed tomography-derived fractional flow reserve: a systematic review. JAMA Cardiol 2:803–810
2. Nous FMA, Budde RPJ, Lubbers MM et al (2020) Impact of machine-learning CT-derived fractional flow reserve for the diagnosis and management of coronary artery disease in the randomized CRESCENT trials. Eur Radiol 30:3692–3701
3. Tsugu T, Tanaka K, Belsack D et al (2021) Impact of vascular morphology and plaque characteristics on computed tomography derived fractional flow reserve in early stage coronary artery disease. Int J Cardiol 343:187–193
4. Cami E, Tagami T, Raff G et al (2018) Assessment of lesion-specific ischemia using fractional flow reserve (FFR) profiles derived from coronary computed tomography angiography (FFRCT) and invasive pressure measurements (FFRINV): importance of the site of measurement and implications for patient referral for invasive coronary angiography and percutaneous coronary intervention. J Cardiovasc Comput Tomogr 12:480–492
5. Tsugu T, Tanaka K, Nagatomo Y et al (2023) Impact of coronary bifurcation angle on computed tomography derived fractional flow reserve in coronary vessels with no apparent coronary artery disease. Eur Radiol 33:1277–1285
6. Tsugu T, Tanaka K (2022) Differences in fractional flow reserve derived from coronary computed tomography angiography according to coronary artery bifurcation angle. Turk Kardiyol Dern Ars 50:83–84
7. Tsugu T, Tanaka K, Belsack D et al (2022) Effects of left ventricular mass on computed tomography derived fractional flow reserve in significant obstructive coronary artery disease. Int J Cardiol 355:59–64
8. Tsugu T, Tanaka K, Belsack D, Jean-Francois A, Mey J (2021) Impact of collateral circulation with fractional flow reserve derived from coronary computed tomography angiography. Turk Kardiyol Dern Ars 49:694–695
9. Gassenmaier S, Tsiflikas I, Greulich S et al (2021) Prevalence of pathological FFRCT values without coronary artery stenosis in an asymptomatic marathon runner cohort. Eur Radiol 31:8975–8982
10. Dodge JT Jr, Brown BG, Bolson EL, Dodge HT (1992) Lumen diameter of normal human coronary arteries. Influence of age, sex, anatomic variation, and left ventricular hypertrophy or dilation. Circulation 86:232–246
11. Collet C, Katagiri Y, Miyazaki Y et al (2018) Impact of coronary remodeling on fractional flow reserve. Circulation 137:747–749
12. Holmes KR, Fonte TA, Weir-McCall J et al (2019) Impact of sublingual nitroglycerin dosage on FFRCT assessment and coronary luminal volume-to-myocardial mass ratio. Eur Radiol 29:6829–6836
13. Cury RC, Abbara S, Achenbach S et al (2016) CAD-RADS(TM) coronary artery disease - reporting and data system. An expert consensus document of the Society of Cardiovascular Computed Tomography (SCCT), the American College of Radiology (ACR) and the North American Society for Cardiovascular Imaging (NASCI). Endorsed by the American College of Cardiology. J Cardiovasc Comput Tomogr 10:269–281
14. Abbara S, Blanke P, Maroules CD et al (2016) SCCT guidelines for the performance and acquisition of coronary computed tomographic angiography: a report of the Society of Cardiovascular Computed Tomography Guidelines Committee: endorsed by the North American Society for Cardiovascular Imaging (NASCI). J Cardiovasc Comput Tomogr 10:435–449
15. Cerqueira MD, Weissman NJ, Dilsizian V et al (2002) Standardized myocardial segmentation and nomenclature for tomographic imaging of the heart. A statement for healthcare professionals from the Cardiac Imaging Committee of the Council on Clinical Cardiology of the American Heart Association. Circulation 105:539–542
16. Tonino PA, De Bruyne B, Pijls NH et al (2009) Fractional flow reserve versus angiography for guiding percutaneous coronary intervention. N Engl J Med 360:213–224
17. Achenbach S, Rudolph T, Rieber J et al (2017) Performing and interpreting fractional flow reserve measurements in clinical practice: an expert consensus document. Interv Cardiol 12:97–109
18. Fairbairn TA, Dobson R, Hurwitz-Koweek L et al (2020) Sex differences in coronary computed tomography angiography-derived fractional flow reserve: lessons from ADVANCE. JACC Cardiovasc Imaging 13:2576–2587
19. Gaur S, Taylor CA, Jensen JM et al (2017) FFR derived from coronary CT angiography in nonculprit lesions of patients with recent STEMI. JACC Cardiovasc Imaging 10:424–433
20. Motoyama S, Sarai M, Harigaya H et al (2009) Computed tomographic angiography characteristics of atherosclerotic plaques subsequently resulting in acute coronary syndrome. J Am Coll Cardiol 54:49–57
21. Nadjiri J, Hausleiter J, Jahnichen C et al (2016) Incremental prognostic value of quantitative plaque assessment in coronary CT angiography during 5 years of follow up. J Cardiovasc Comput Tomogr 10:97–104
22. De Bruyne B, Hersbach F, Pijls NH et al (2001) Abnormal epicardial coronary resistance in patients with diffuse atherosclerosis but "normal" coronary angiography. Circulation 104:2401–2406
23. Tsugu T, Tanaka K, Nagatomo Y, Belsack D, De Maeseneer M, De Mey J (2022) Paradoxical changes of coronary computed tomography derived fractional flow reserve. Echocardiography 39:398–403
24. Tsugu T, Tanaka K, Nagatomo Y et al (2023) Impact of ramus coronary artery on computed tomography derived fractional flow reserve (FFR(CT)) in no apparent coronary artery disease. Echocardiography 40:103–112.
25. Pfitzner J (1976) Poiseuille and his law. Anaesthesia 31:273–275

26. Baumgartner H, Stefenelli T, Niederberger J et al (1999) "Overestimation" of catheter gradients by Doppler ultrasound in patients with aortic stenosis: a predictable manifestation of pressure recovery. J Am Coll Cardiol 33:1665–1661
27. Urschel K, Tauchi M, Achenbach S, Dietel B (2021) Investigation of wall shear stress in cardiovascular research and in clinical practice-from bench to bedside. Int J Mol Sci 26;22:5635.
28. Koo BK, Erglis A, Doh JH et al (2011) Diagnosis of ischemia-causing coronary stenoses by noninvasive fractional flow reserve computed from coronary computed tomographic angiograms. Results from the prospective multicenter DISCOVER-FLOW (Diagnosis of Ischemia-Causing Stenoses Obtained Via Noninvasive Fractional Flow Reserve) study. J Am Coll Cardiol 58:1989–1997
29. Douglas PS, Pontone G, Hlatky MA et al (2015) Clinical outcomes of fractional flow reserve by computed tomographic angiography-guided diagnostic strategies vs. usual care in patients with suspected coronary artery disease: the prospective longitudinal trial of FFR(CT): outcome and resource impacts study. Eur Heart J 36:3359–3367
30. Min JK, Taylor CA, Achenbach S et al (2015) Noninvasive fractional flow reserve derived from coronary CT angiography: clinical data and scientific principles. JACC Cardiovasc Imaging 8:1209–1222
31. Gaur S, Ovrehus KA, Dey D et al (2016) Coronary plaque quantification and fractional flow reserve by coronary computed tomography angiography identify ischaemia-causing lesions. Eur Heart J 37:1220–1227
32. Otaki Y, Han D, Klein E et al (2022) Value of semiquantitative assessment of high-risk plaque features on coronary CT angiography over stenosis in selection of studies for FFRct. J Cardiovasc Comput Tomogr 16:27–33
33. Driessen RS, Stuijfzand WJ, Raijmakers PG et al (2018) Effect of plaque burden and morphology on myocardial blood flow and fractional flow reserve. J Am Coll Cardiol 71:499–509
34. Chaichana T, Sun Z, Jewkes J (2010) Computation of hemodynamics in the left coronary artery with variable angulations. J Biomech 44:1869–1878